DNA-TR-86-243-V5

EFFECTS FOR ICBM BASING

Volume V—Flow Field Modeling

David P. Bacon
Science Applications International Corporation
P. O. Box 1303
McLean, VA 22102-1303

31 December 1985

Technical Report

CONTRACT No. DNA 001-84-C-0130

THIS WORK WAS SPONSORED BY THE DEFENSE NUCLEAR AGENCY
UNDER RDT&E RMSS CODE B344084466 Y99QMXSG00021 H2590D.

Prepared for
Director
DEFENSE NUCLEAR AGENCY
Washington, DC 20305-1000

UNCLASSIFIED

SECURITY CLASSIFICATION OF THIS PAGE

REPORT DOCUMENTATION PAGE

Form Approved
OMB No. 0704-0188
Exp. Date: Jun 30, 1986

1a. REPORT SECURITY CLASSIFICATION UNCLASSIFIED	1b. RESTRICTIVE MARKINGS
2a. SECURITY CLASSIFICATION AUTHORITY N/A since Unclassified	3. DISTRIBUTION / AVAILABILITY OF REPORT
2b. DECLASSIFICATION / DOWNGRADING SCHEDULE N/A since Unclassified	
4. PERFORMING ORGANIZATION REPORT NUMBER(S) SAIC 85/1742	5. MONITORING ORGANIZATION REPORT NUMBER(S) DNA-TR-86-243-V5
6a. NAME OF PERFORMING ORGANIZATION Science Applications International Corporation 6b. OFFICE SYMBOL (If applicable)	7a. NAME OF MONITORING ORGANIZATION Director Defense Nuclear Agency
6c. ADDRESS (City, State, and ZIP Code) P. O. Box 1303 McLean, VA 22102-1303	7b. ADDRESS (City, State, and ZIP Code) Washington, DC 20305-1000
8a. NAME OF FUNDING / SPONSORING ORGANIZATION 8b. OFFICE SYMBOL (If applicable)	9. PROCUREMENT INSTRUMENT IDENTIFICATION NUMBER DNA 001-84-C-0130
8c. ADDRESS (City, State, and ZIP Code)	10. SOURCE OF FUNDING NUMBERS PROGRAM ELEMENT NO. 62715H; PROJECT NO Y99QMXS; TASK NO G; WORK UNIT ACCESSION NO. DH008212

11. TITLE (Include Security Classification)
EFFECTS OF ICBM BASING
Volume V—Flow Field Modeling

12. PERSONAL AUTHOR(S)
Bacon, David P.

13a. TYPE OF REPORT	13b. TIME COVERED	14. DATE OF REPORT (Year, Month, Day)	15. PAGE COUNT
Technical	FROM 831230 TO 850430	851231	

16. SUPPLEMENTARY NOTATION
This work was sponsored by the Defense Nuclear Agency under RDT&E RMSS Code B344084466 Y99QMXSG00021 H2590D.

17. COSATI CODES		
FIELD	GROUP	SUB-GROUP
18	3	
16	1	

18. SUBJECT TERMS (Continue on reverse if necessary and identify by block number)
Meteorology
Nuclear Weapons Effects
Nuclear Winter

19. ABSTRACT (Continue on reverse if necessary and identify by block number)

The effect of the ambient meteorology (temperature and dewpoint profiles) on the dynamics of a rising fireball and the plume from a large-area fire (firestorm) has been studied. The primary results indicate the importance of moisture for both phenomena and indicates that the ambient meteorology may grossly affect cloud stabilization and precipitation. The role of precipitation and its resultant scavenging remains to be investigated.

20 DISTRIBUTION / AVAILABILITY OF ABSTRACT ☒ UNCLASSIFIED/UNLIMITED ☐ SAME AS RPT ☐ DTIC USERS	21 ABSTRACT SECURITY CLASSIFICATION UNCLASSIFIED
22a NAME OF RESPONSIBLE INDIVIDUAL Betty L. Fox	22b TELEPHONE (Include Area Code) (202) 325-7042 22c. OFFICE SYMBOL DNA/STTI

DD FORM 1473, 84 MAR 83 APR edition may be used until exhausted
All other editions are obsolete.

SECURITY CLASSIFICATION OF THIS PAGE
UNCLASSIFIED

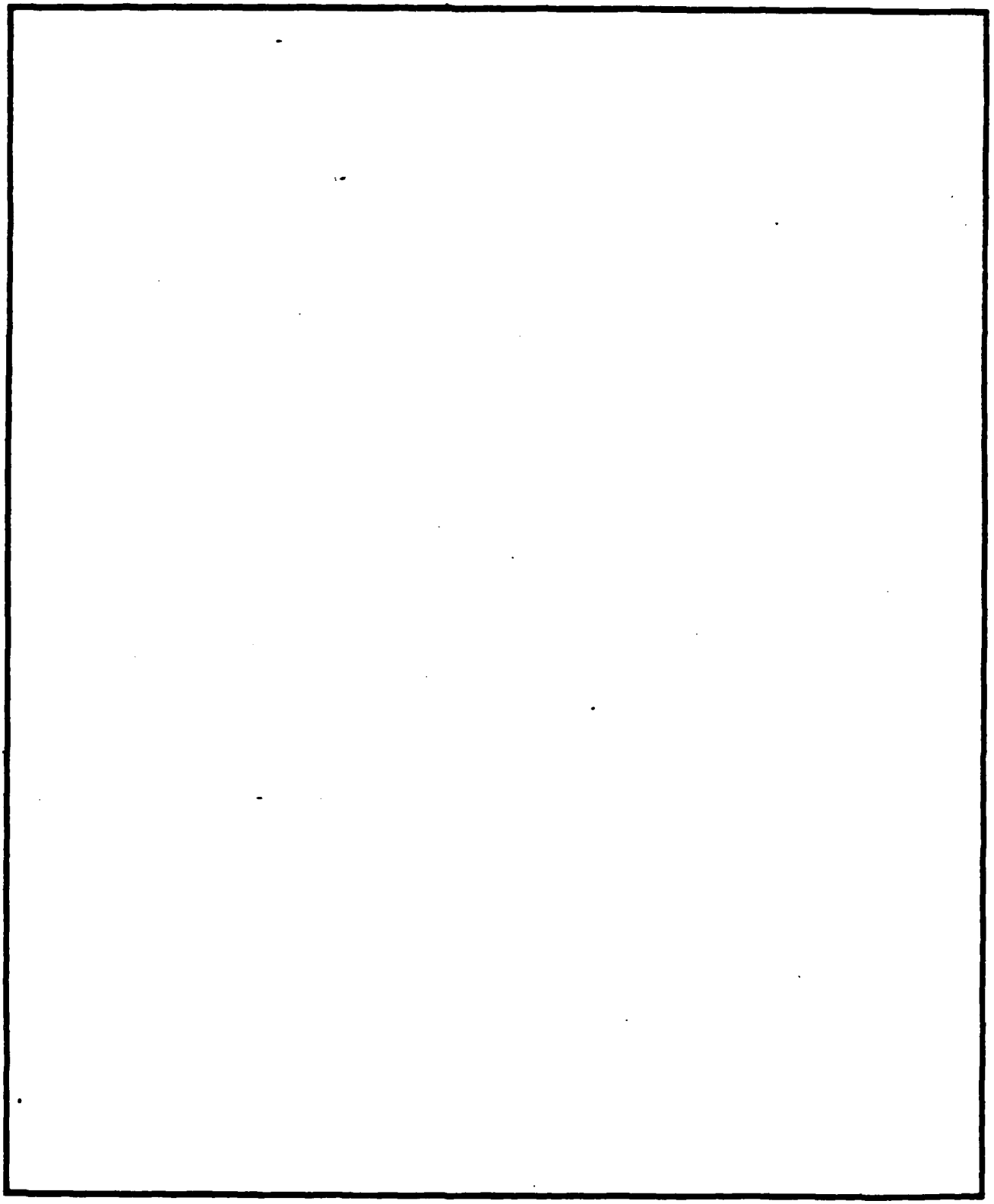

EXECUTIVE SUMMARY

In an attempt to bring a new capability to the problem of nuclear fireball rise and the dynamics of the plumes from nuclear-burst induced firestorms, a joint program of SAIC and NASA/LaRC and their contractor Systems and Applied Sciences Corporation (SASC) was launched. This program centered on modifying and applying the Terminal Area Simulation System (TASS) to the above problems. The result of this effort is a new research tool for use in the study of nuclear weapons effects problems.

TASS was used to study the effects of the ambient meteorology (temperature and dewpoint profiles) on the dynamics of both rising fireballs and the plume from a large area fire or firestorm. In addition, it was used to investigate the effect of the spatial distribution and time history of the fire on the dynamics and the stabilization of the resulting cloud. The preliminary results indicate that the cloud stabilization is not sensitive to either the spatial distribution of the fire or to its time history, but rather is interested in the total energy input to the atmosphere by the fire. On the other hand, the stabilization is strongly dependent on the ambient meteorology, especially the amount of moisture present.

Even though we have not exhausted the study of the effect of the ambient meteorology, we have identified two new areas of research that may also be important: three-dimensional effects and the effect of scavenging of particulates by precipitation. These research areas should constitute the core of a continuing program.

CONVERSION TABLE

Conversion factors for U.S. Customary to metric (SI) units of measurement

MULTIPLY →	BY →	TO GET
TO GET ←	BY ←	DIVIDE
angstrom	1.000 000 X E -10	meters (m)
atmosphere (normal)	1.013 25 X E +2	kilo pascal (kPa)
bar	1.000 000 X E +2	kilo pascal (kPa)
barn	1.000 000 X E -28	meter^2 (m^2)
British thermal unit (thermochemical)	1.054 350 X E +3	joule (J)
calorie (thermochemical)	4.184 000	joule (J)
cal (thermochemical)/cm^2	4.184 000 X E -2	mega joule/m^2 (MJ/m^2)
curie	3.700 000 X E +1	*giga becquerel (GBq)
degree (angle)	1.745 329 X E -2	radian (rad)
degree Fahrenheit	t_k = (t°f + 459.67)/1.8	degree kelvin (K)
electron volt	1.602 19 X E -19	joule (J)
erg	1.000 000 X E -7	joule (J)
erg/second	1.000 000 X E -7	watt (W)
foot	3.048 000 X E -1	meter (m)
foot-pound-force	1.355 818	joule (J)
gallon (U. S. liquid)	3.785 412 X E -3	meter^3 (m^3)
inch	2.540 000 X E -2	meter (m)
jerk	1.000 000 X E +9	joule (J)
joule/kilogram (J/kg) (radiation dose absorbed)	1.000 000	Gray (Gy)
kilotons	4.183	terajoules
kip (1000 lbf)	4.448 222 X E +3	newton (N)
kip/inch^2 (ksi)	6.894 757 X E +3	kilo pascal (kPa)
ksap	1.000 000 X E +2	newton-second/m^2 (N-s/m^2)
microm	1.000 000 X E -6	meter (m)
mil	2.540 000 X E -5	meter (m)
mile (international)	1.609 344 X E +3	meter (m)
ounce	2.834 952 X E -2	kilogram (kg)
pound-force (lbf avoirdupois)	4.448 222	newton (N)
pound-force inch	1.129 848 X E -1	newton-meter (N-m)
pound-force/inch	1.751 268 X E +2	newton/meter (N/m)
pound-force/foot^2	4.788 026 X E -2	kilo pascal (kPa)
pound-force/inch^2 (psi)	6.894 757	kilo pascal (kPa)
pound-mass (lbm avoirdupois)	4.535 924 X E -1	kilogram (kg)
pound-mass-foot^2 (moment of inertia)	4.214 011 X E -2	kilogram-meter^2 (kg-m^2)
pound-mass/foot^3	1.601 846 X E +1	kilogram/meter^3 (kg/m^3)
rad (radiation dose absorbed)	1.000 000 X E -2	**Gray (Gy)
roentgen	2.579 760 X E -4	coulomb/kilogram (C/kg)
shake	1.000 000 X E -8	second (s)
slug	1.459 390 X E +1	kilogram (kg)
torr (mm Hg, 0° C)	1.333 22 X E -1	kilo pascal (kPa)

*The becquerel (Bq) is the SI unit of radioactivity; 1 Bq = 1 event/s.
**The Gray (Gy) is the SI unit of absorbed radiation.

TABLE OF CONTENTS

LIST OF ILLUSTRATIONS

LIST OF TABLES

Page viii intentionally left blank and not included.

SECTION 1
INTRODUCTION

In the past, the calculation of fireball rise has been performed with one of two classes of code: phenomenological or first-principles shock/hydrodynamic. The former was fixed to the DNA 1 KT standard and then scaled in various ways; the latter attempted to resolve the shock physics for the developing fireball and then followed the buoyant rise thereof. Neither approach is acceptable. The former can be shown to yield numbers of little use to investigators requiring detailed information on the fireball, and the latter requires an inordinately large amount of computer time to study the late-time (~1 min) fireball rise.

The primary problems with employing a shock/hydrodynamic code to the phenomenon of fireball rise are three: (1) once the shock has propagated out of the computational domain (T of the order of 100 sec), the high resolution of the shock code is not needed and serves as a huge computational overhead (even before this time the shock has decayed sufficiently to be treated as an acoustic wave and shock resolution is not strictly necessary); (2) most shock/hydro codes are inviscid and while this approximation is valid during the period that the shock physics dominates, the fireball rise problem depends a great deal on the turbulence and entrainment processes and therefore on the viscosity; (3) none of the shock hydrocodes to date has considered the effect of the meteorology (temperature and dewpoint profile) on the fireball rise.

In an attempt to circumvent the above problems, SAIC, in collaboration with NASA/LaRC and their contractor Systems and Applied Sciences Corporation (SASC), has been working to modify a non-hydrostatic meteorological code, the Terminal Area Simulation System (TASS) to allow for the study of nuclear fireball rise and the study of the dynamics of plumes from large area fires and firestorms. The reason that such a code was deemed suitable for these problems is that as a non-hydrostatic code, it retains the acoustic pressure waves and therefore while it is not capable of capturing and retaining a shock wave, after approximately 30 seconds, the shock from a nuclear cloud is traveling at the speed of sound and is weak enough to be considered to be a simple acoustic wave. In addition, since TASS is a meteorological code, it has inherently in it the cloud microphysics and hydrometeor formation and growth

processes that are significant if one wants to understand the water and ice problem. The fact that this is a much more efficient algorithm allows us to investigate many more scenarios than is possible with a shock/hydro code.

During the past year, SAIC performed a large number of simulations of rising fireballs and the plumes from large area fires. In this report we will document a few of the calculations performed. First, however, we present a brief synopsis of TASS and some of the validation studies performed on it.

SECTION 2
THE TERMINAL AREA SIMULATION SYSTEM (TASS)

The Terminal Area Simulation System (TASS) is a non-hydrostatic computer code originally developed by Fred Proctor of SASC to model the development of strong isolated convective activity. The code contains parameterizations for the formation and size distribution of both precipitating and non-precipitating hydrometeors: rain, hail, snow and cloud water and ice. This parameterization includes the release of the latent heat of condensation and solidification as well as the main interactions between the various classes of hydrometeors. Table 1 contains an overview of the basic features of the code.

Various tests have been performed to see the effect of the grid size and the boundary conditions on the simulations to be reported below. Figure 1 shows the effect of the boundary conditions on the simulations reported. The top figure shows the smoke contours at 20 minutes into a large area fire simulation run over a 30 km x 30 km domain with a 1/3 km grid resolution; the bottom figure represents the same simulation run over a 15 km x 15 km domain. This figure very nicely shows the lack of interaction with the lateral boundary.

In a similar vein, Figure 2 shows a comparison of the same simulation as above run with grid resolutions of 0.1, 1/3, and 1 km. Because of the differing contour levels, one must look at particular concentration contours in order to evaluate the differences between the three simulations. Table 2 shows an evaluation of two different contour levels.

Table 1. The terminal area simulation system (TASS).

Prognostic Equations for:	Momentum Pressure Potential Temperature Water Vapor Cloud Water Cloud Ice Rain Snow Hail Smoke (Massless Tracer)
Turbulence Closure:	Smagorinsky - depends on stratification and shear
Boundary Conditions:	Surface - Nonslip velocity - Continuous thermodynamics - Time-dependent surface heat source Axial - Symmetric for all variables Lateral - Open boundary for all variables Radiative wave speeds from interior points Top - Zero vertical velocity Constant potential temperature All other variables continuous
Parameterizations:	Autoconversion of cloud water into rain Accretion of cloud water by rain Evaporation of rain Spontaneous freezing of supercooled cloud water and rain Initiation of cloud ice Accretion of cloud water by cloud ice Autoconversion of cloud ice into hail Deposition and sublimination of hail and cloud ice Accretion of cloud water and cloud ice by hail Freezing of rain due to the collision of cloud ice and supercooled rain Shedding of unfrozen water by hail Initiation of snow Accretion of cloud water by snow Melting of cloud ice, snow, and hail
Additional Diagnostics:	Radar reflectivity Hydrometeor concentrations

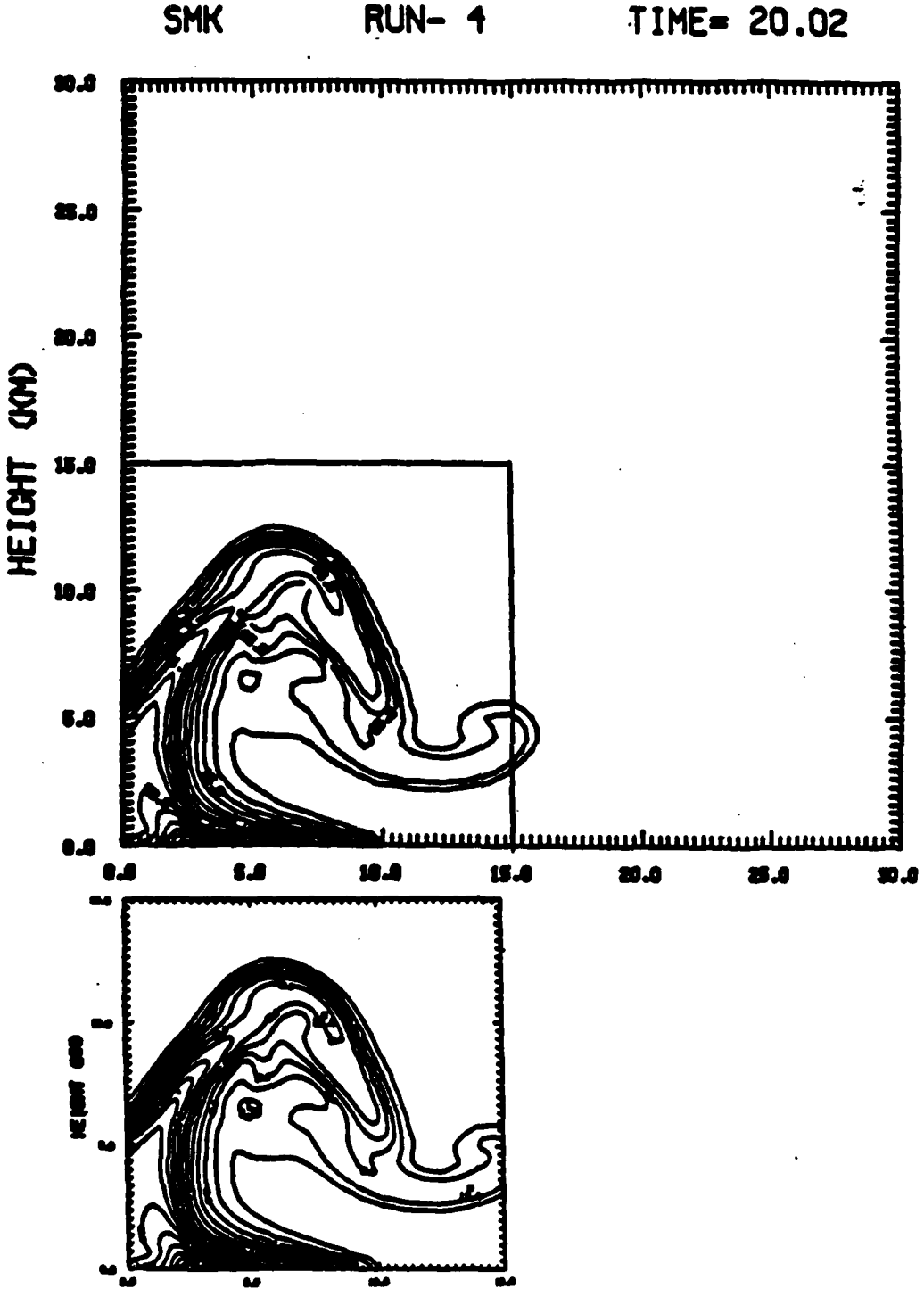

Figure 1. Test of boundary conditions using 30 x 30 km domain (top) and 15 x 15 km domain (bottom).

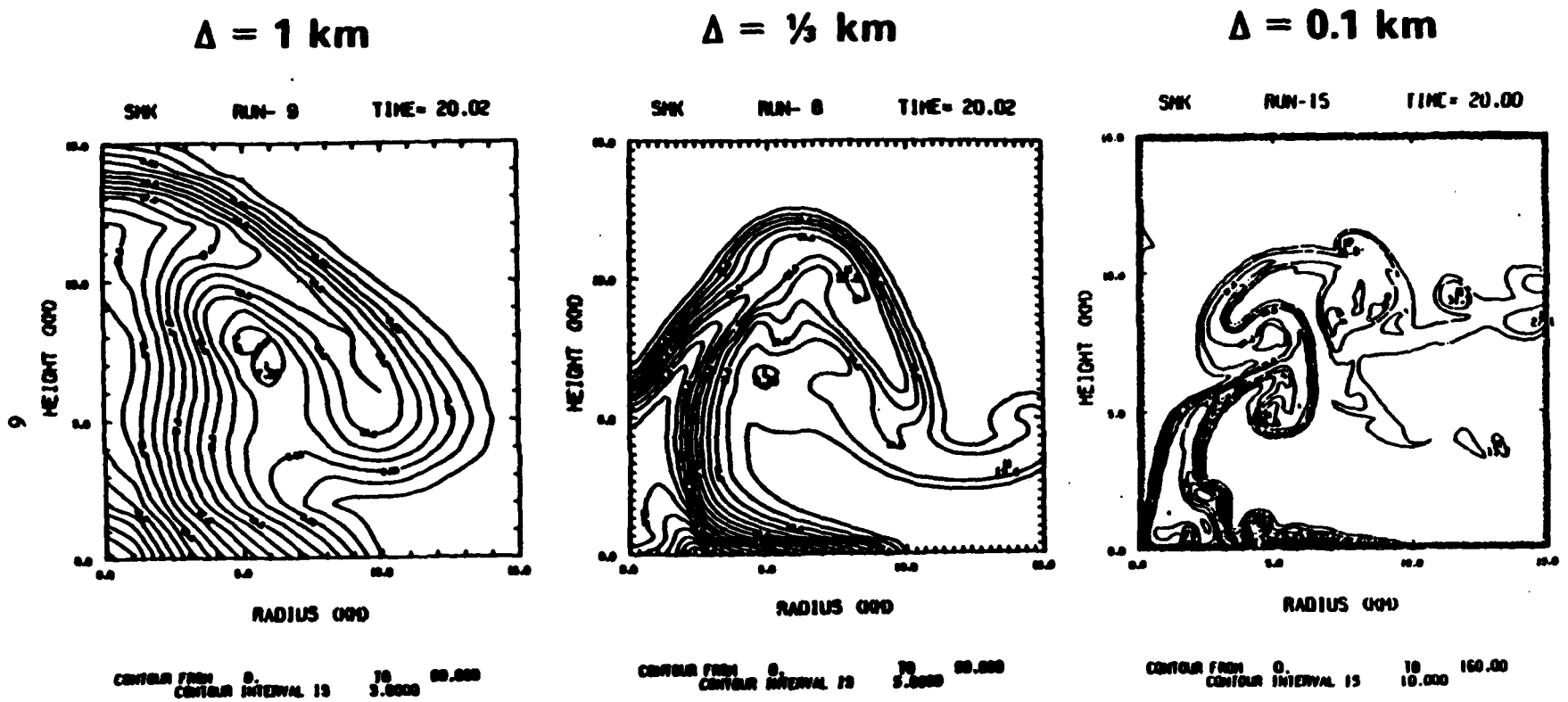

Figure 2. Smoke contours for 10 km baseline fire using a 1 km (left), 1/3 km (center), and 0.1 (right) grid resolution.

Table 2. TASS grid resolution test cases.

Grid Size (km)	Maximum Height of Contour (km)	
	15	30
0.1	11.5	10.5
0.3	12.0	11.7
1.0	14.0	13.0

Thus we see that increasing the grid size by a factor of 10 results in only a 25% increase in the maximum altitude of the smoke tracers in these simulations. Since the computation time increases with the number of computational cells, for our production runs we used a 1.0 km grid cell; for special runs, we employed a 0.5 km grid cell.

One other point should be noted in Figure 2 and Table 2: the region of non-agreement between the different cases is mostly near the axis. This is because any code with axial symmetry has a problem handling diffusion and entrainment at the axis. This is one of the reasons why we felt that we needed to expand the code to three-dimensions, a process which is ongoing at NASA.

In Appendix A we include a complete set of the diagnostics produced by TASS at one point in time for one of the large-area fire simulations described in Section IV below. This set includes: the relative humidity (%), RLH; the radial, U, and vertical, w, velocities (m/s); the temperature deviation (^{o}C); the streamlines, PSI; the pressure deviation, P; the rain, XIP, hail, XIH, and total, XIT, precipitation (g/kg); the radar reflectivity, RRF; the equivalent potential temperature, EPOT; and the massless tracer, SMK.

8 Blank

SECTION 3
FIREBALL SIMULATIONS

Early in the contract period, two simulations of a fireball rise were performed; one using a sounding from Marfa, TX, the other a sounding taken 5 hours later in Lake Charles, LA. The Marfa sounding was dry and had a tropopause at approximately 11.0 km while the Lake Charles sounding was very wet (with 1.63" of precipitable water vapor) and had a tropopause at approximately 13.5 km. The two simulations were initiated by adding a thermal "bubble" of overtemperature at the surface. The bubble was hemispherical and had a peak overtemperature of 100°C and was intended to represent the thermal energy of a nuclear burst of yield O(1 MT). Figure 3 shows the relative humidity profiles from these simulations. (These simulations were run with a 0.5 km grid size.) As can be seen, the visible cloud (represented by the 100% relative humidity - the innermost contour) at 5 minutes is 3.5 km higher in the wet sounding than in the dry sounding. Part of this difference may be due to the different levels of the tropopause, but part of it is due to the release of the latent heats of condensation and fusion.

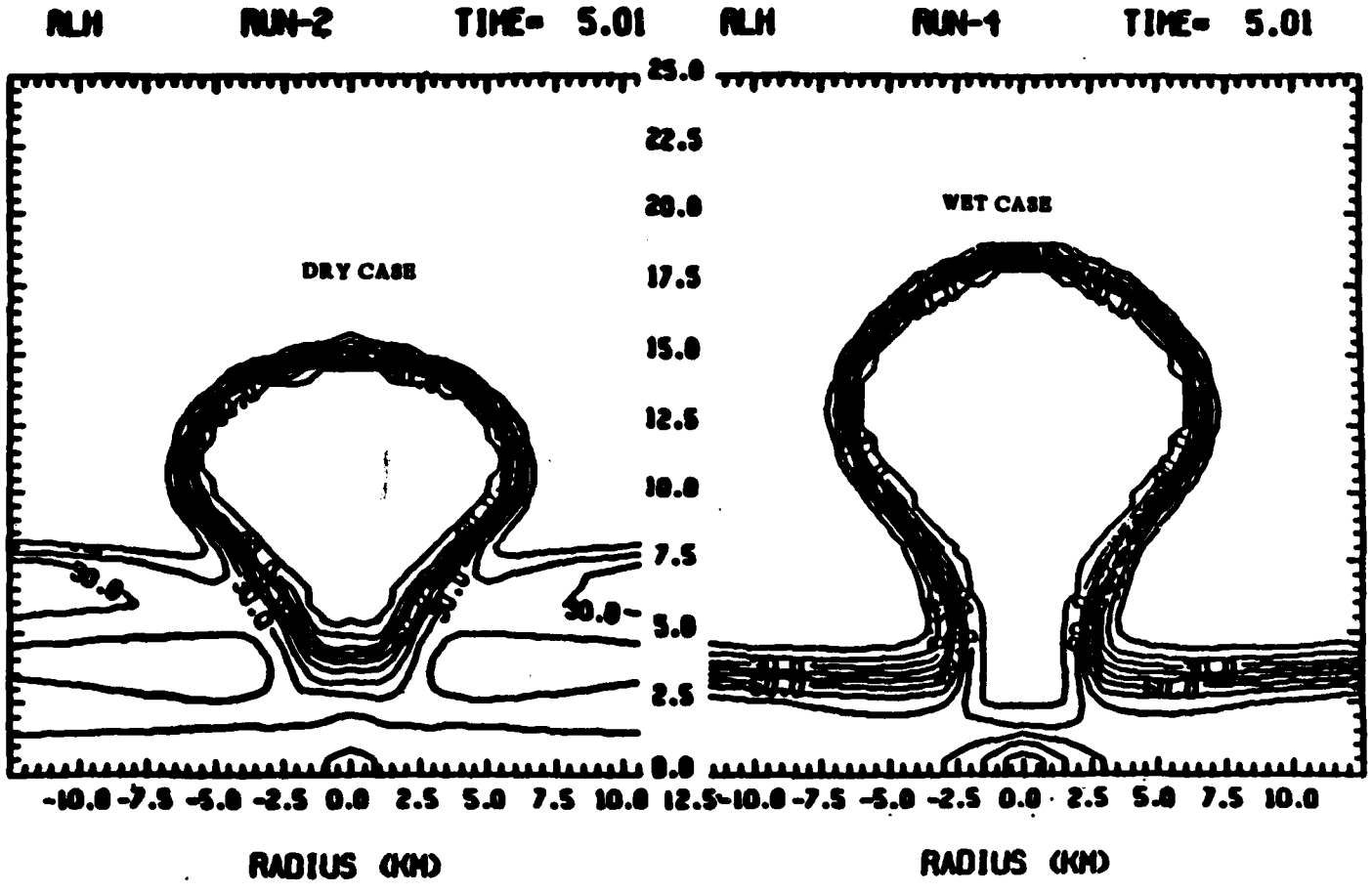

Figure 3. Rise of a 100°C thermal bubble (fireball) in two different soundings: a dry mafa, TX case (left) and a wet Lake Charles, LA case (right).

SECTION 4
LARGE-AREA FIRE SIMULATIONS

A large number of simulations were performed on the response of the atmosphere to a perturbation resembling that of a large area fire. These simulations used a 1 km grid size and were performed for a variety of fire intensities, sizes, spatial distributions, time histories and for a variety of atmospheric soundings. Since so many cases have been run, we have selected just a few to discuss in detail. In Table 3 we present an overview of the results of many of the simulations.

Case 1 (Designated Run-0): This was our baseline case. The atmospheric sounding is the same Lake Charles sounding mentioned above and is a moist, unstable atmosphere. The fire was a uniform 10 km radius which started cold at time T=0 and rose linearly in time to a peak power density of 0.25 MW/m^2 (for a total power input of roughly 8×10^{13} W) in 15 minutes. The fire maintained this intensity for 30 minutes and then linearly decayed to zero in 15 minutes. Thus at 1 hour into the simulation, the fire was out. Over its 1 hour duration, the fire provided 2×10^{17} J (which is equivalent to 50 MT) of thermal energy.

In Figure 4, we show the smoke tracer for this fire at times 10, 30, 50, and 70 minutes. At 10 minutes into the simulation, the fire has not reached its peak intensity and the smoke is confined to a disk shaped region approximately 4 km in height by 10 km in radius. By 30 minutes into the simulation, the smoke plume has reached an altitude of 25 km and a radius of 33 km. Three factors have caused this rapid growth in the plume: (1) the fire heat source achieved its maximum intensity at T=15 minutes and has been providing a strong thermal input; (2) the moisture lofted by the addition of heat reached the saturation point and condensed providing an additional thermal input due to the release of latent heat; and (3) the upwelling air mass has associated with it a strong radial outflow at altitude (and a radial inflow near the surface) which carries the smoke with it. Other than "filling in", little change occurs in the cloud over the next 20 minutes. The fire is beginning its decay phase but is still supplying a considerable amount of heat and smoke to the atmosphere. By 70 minutes, with the fire now out, the plume begins to decay with the smoke forming a band between 9 and 21 km.

Table 3. Summary of TASS firestorm calculations.

	Max Smoke Height (km)	
	30 Min (Peak)	70 Min (Wings)
Spatial Study - LCH (13.9 km Tropopause) / 51 Mt Thermal Input		
10 km Uniform	25	9-21
6-10 km Annulus	19	9-19
Peak on Axis	25	13-19
Peak at Edge	20	9-21
Temporal Study - LCH (13.9 km Tropopause) / 51 Mt Thermal Input		
Baseline	25	9-21
Fast Burn	31	9-20
Combined Study - LCH / 2 Mt Thermal Input		
2 km Baseline	18	12-15
6 km Trigger	17	12-15

Sounding Study - 51 Mt

Sounding	Tropopause (km)		
LCH	13.9	25	9-21
DRY	13.9	20	5-9
SCL	9.2	15	8-11

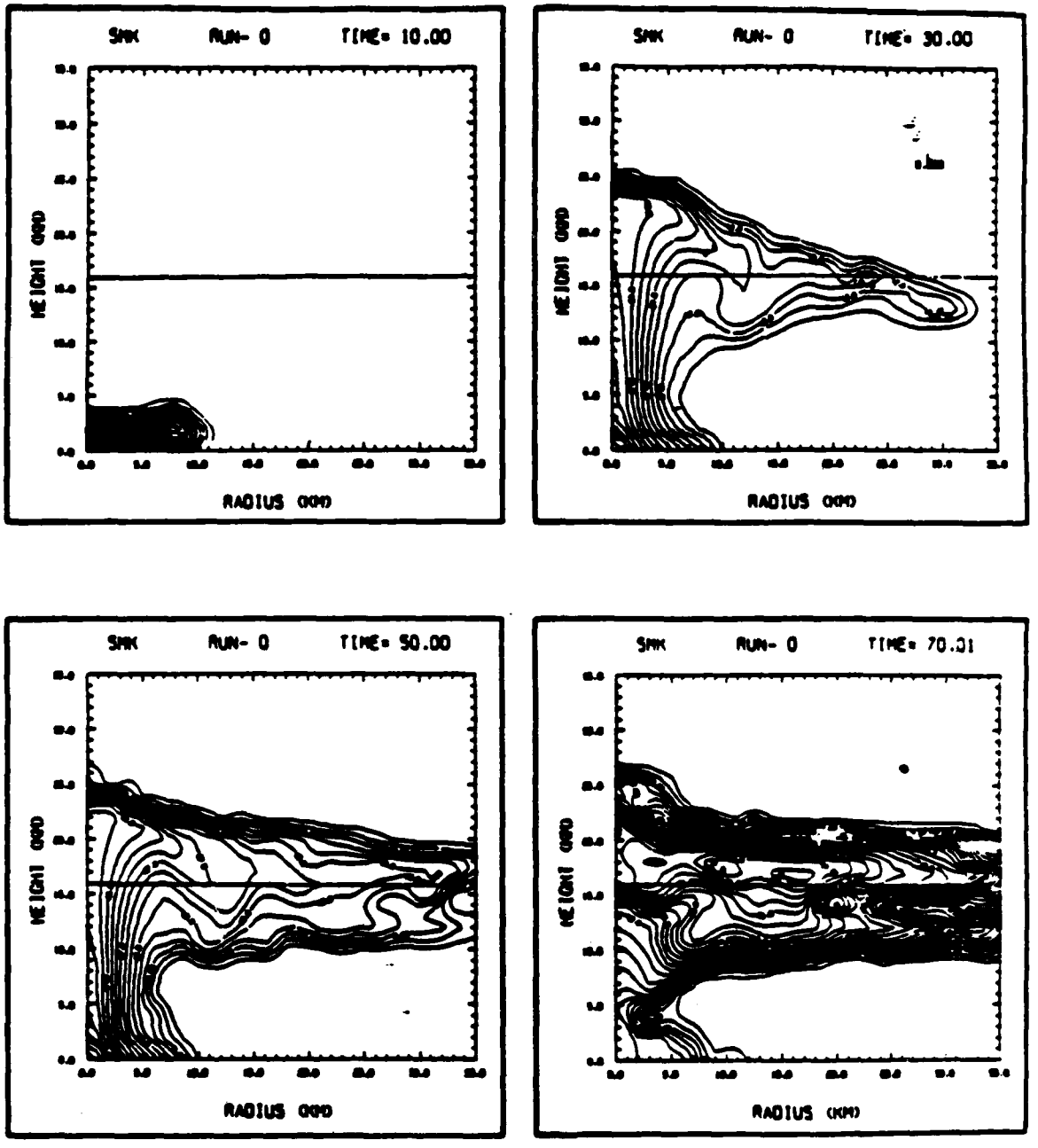

Figure 4. Baseline large area fire simulation - smoke contours.

Case 2 (Run-1): This case is the most extreme of the cases run varying the fire spatial distribution (MW/m^2) while keeping the total power (MW) the same. The fire was uniform, but over an annulus from 6 to 10 km. The time history (15 minute rise, 30 minute plateau, 15 minute decay) was the same, however, in order to keep the same total power, the peak intensity was increased from 0.25 to 0.39 MW/m^2. As might be expected, the early and mid-time smoke plumes show a considerable change from our baseline case. This is due in part to the early formation of a downward flow on axis which takes some time to overcome. The post-fire plume, however, is remarkably similar to the baseline case with the smoke stabilizing in a 9-19 km band. Figure 5 compares the 10 and 70 minute smoke contours for the uniform and annular fires. In all four simulation investigations the effect of the spatial distribution, the post-fire smoke stabilized within a band from 9-21 km.

Case 3 (Run-100): This case explored the effect of varying the fire time history while keeping the same total energy input (50 MT thermal). We reverted to our baseline fire spatial distribution (uniform, 10 km radius) but the fire time history consisted of a "fast burn" followed by a "smoldering fire". This fire ramped in 5 minutes to 0.075 MW/m^2 and then in the next 5 minutes climbed to 0.75 MW/m^2. This intensity remained for 5 minutes followed by a decay to 0.15 MW/m^2 over the following 5 minutes. The fire then decayed to zero over the next 40 minutes.

This simulation has some striking features. At 10 minutes, even though the fire has reached its peak intensity, the atmosphere has not had time to respond; in addition, the "bow wave" of the air above the axis has a strong resistance to the rising air mass. (This may be caused by the forced axial symmetry of the simulation.) However, a look at the comparison presented in Figure 6 shows that by 30 minutes the intense fire period has served to loft smoke to an altitude of 30 km where the baseline peak altitude was 25 km. (This increase may also be a figment of the forced axisymmetry which reduces the entrainment on axis.) This shows the sensitivity over short periods of time of the plume to the total fire intensity. A look at the smoke at 70 minutes on the other hand shows that it has stabilized in a band from 9-20 km, the same band as the baseline study. This indicates that while the short-time atmospheric response may depend on the fire intensity, the long time response is only a function of the total thermal energy input.

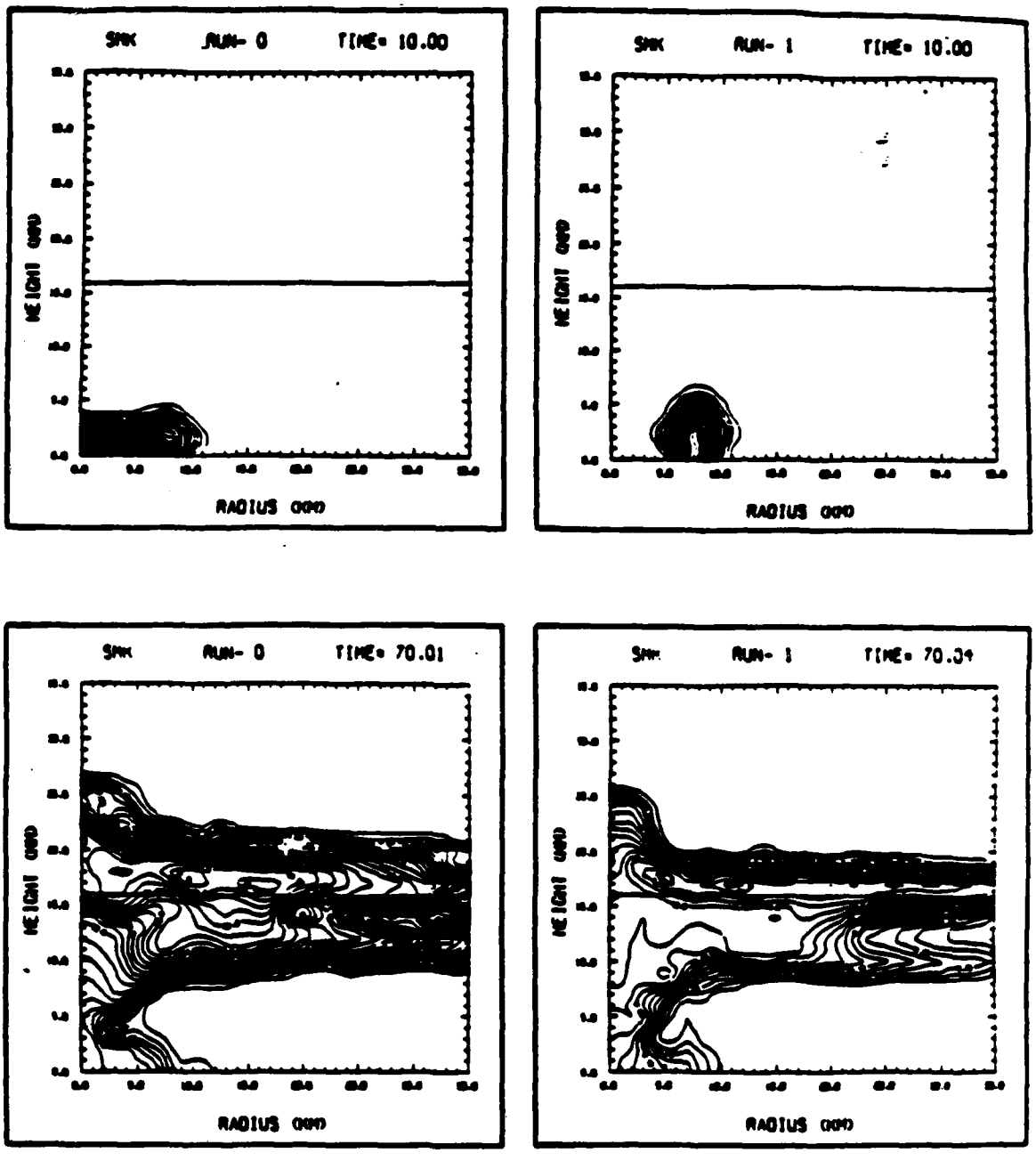

Figure 5. Comparison of smoke contours for baseline simulation (left) and annular fire (right).

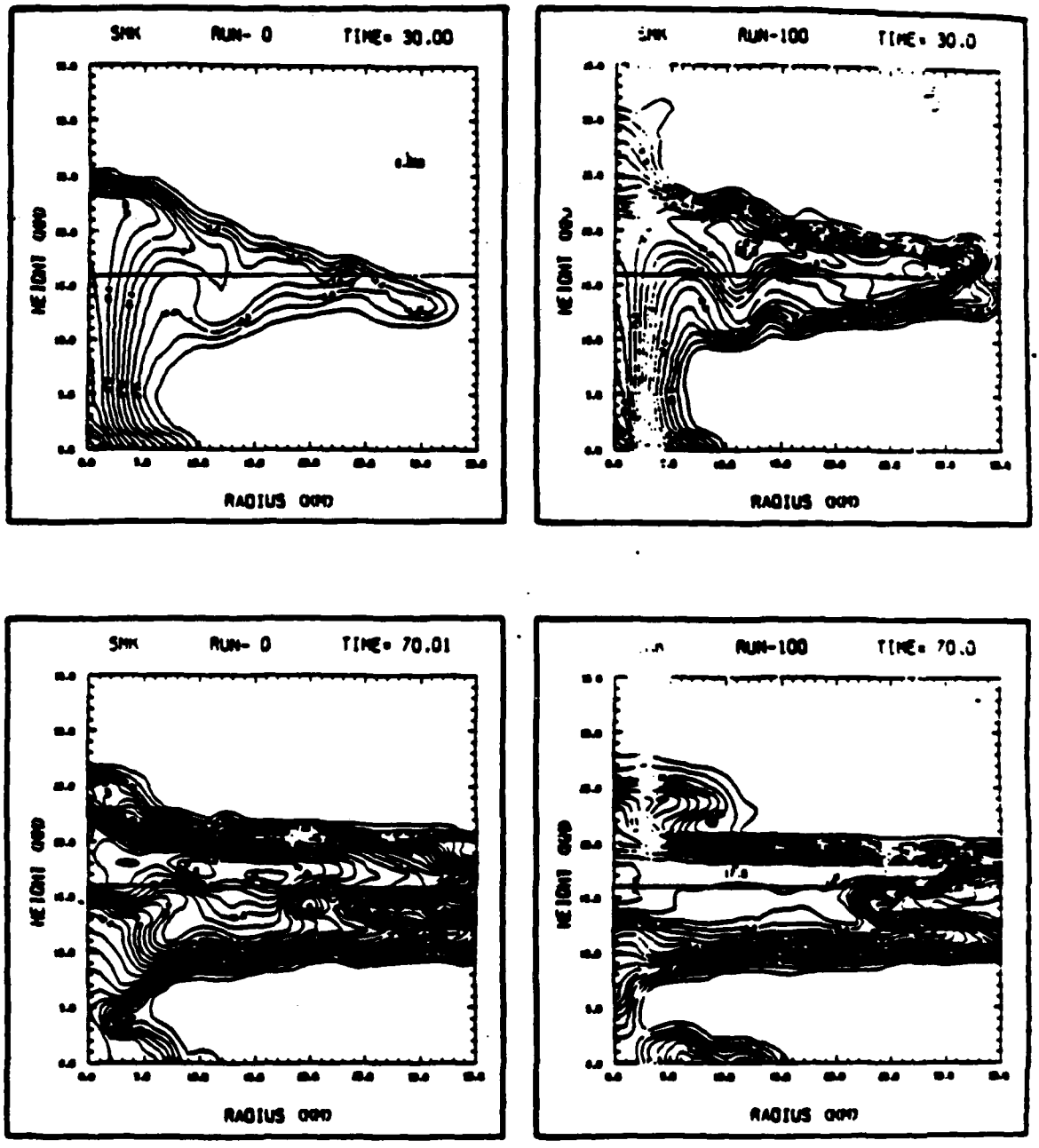

Figure 6. Comparison of smoke contours for baseline simulation (left) and fast burn/smoldering fire (right).

This last observation may be due in part to the fact that we are overdriving the atmosphere to the point that the cloud dynamics are being driven by the latent heat release. During these simulations, more energy was released due to condensation and solidification than was input by the fire; in addition the latent heat release occurred where it would have the most impact on the smoke lofting - in the cloud itself.

Case 4 (Run-900): In order to explore the effect of the latent heat release, we repeated the baseline case with the same Lake Charles temperature profile but with no moisture. Figure 7 shows a side-by-side comparison of the baseline fire with (left) and without (right) moisture. As is obvious, the moisture content of the atmosphere plays a crucial role in the cloud dynamics. For this reason, the use of a standard (dry) atmosphere for these type of calculations should be avoided.

Triggering Cases: As a final series of simulations, we explored the amount of energy required to "trigger" convective activity for the unstable Lake Charles sounding. Figure 8 shows the 70 minute smoke clouds for four different fire space and time distributions. The upper left plot shows the smoke contours resulting from a 2 km radius "triggering" fire. (A "triggering" fire turns on at time T=10 minutes, peaks at T=15 minutes, and ends at T=20 minutes.) This fire deposits 225 kT of (thermal) energy into the atmosphere. Compare this case to the two cases shown on the right hand side of Figure 8: the upper plot shows the 70 minute smoke from a 2 km radius fire with the full baseline (1 hour duration) time history; the lower plot shows the mode from a 6 km radius fire with a "triggering" time history. Each of these cases deposits 2 MT of energy. The final case shown (lower left) is a 10 km radius "triggering" fire which deposits roughly 5.6 MT of energy into the atmosphere.

The significance of these runs is that they span a factor of 20 in input energy and yet in all cases the smoke reached the tropopause. This is good evidence that more attention needs to be paid to the ambient meteorology in this type of simulation.

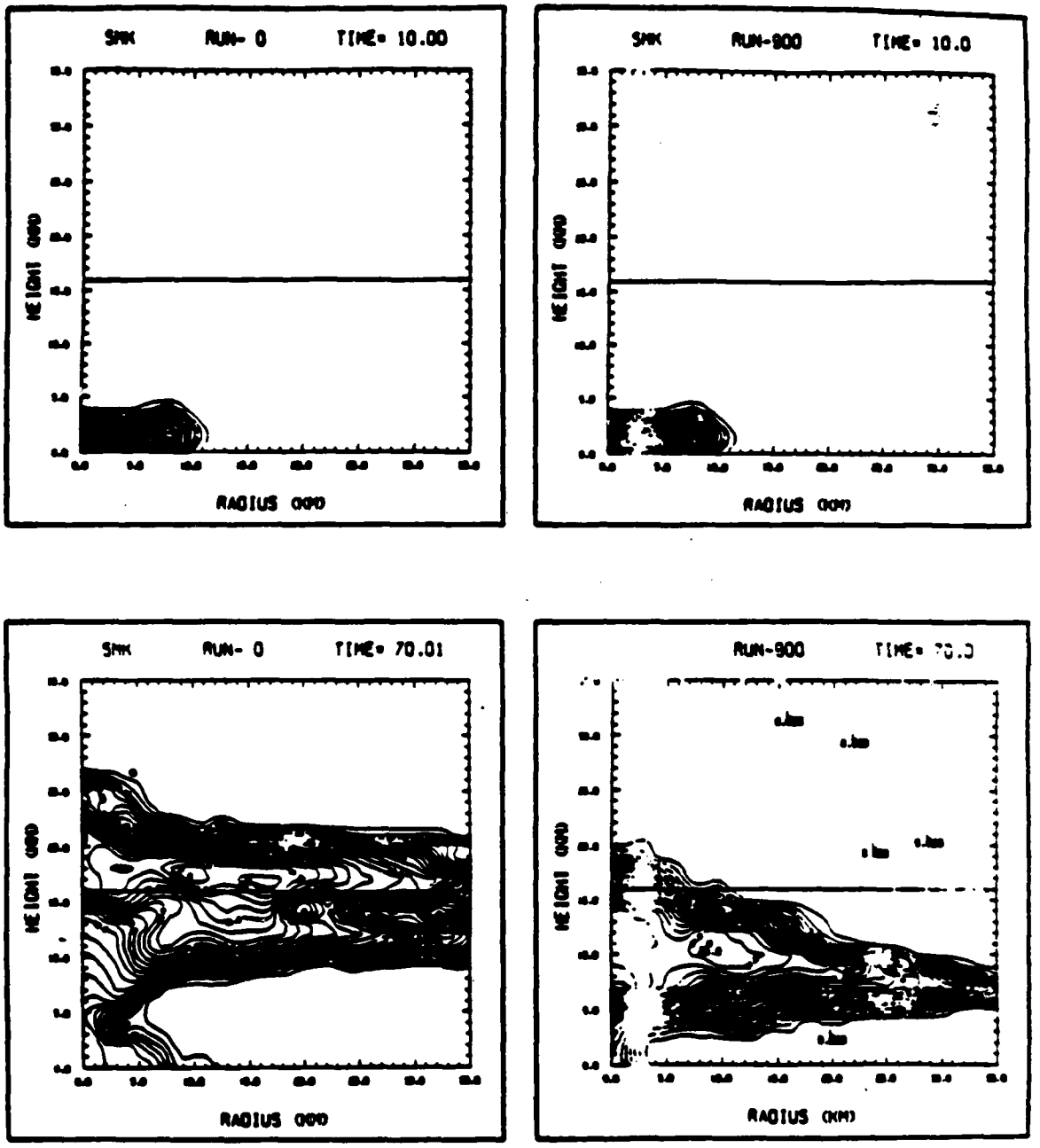

Figure 7. Comparison of smoke for baseline simulation (left) and dry atmosphere simulation (right).

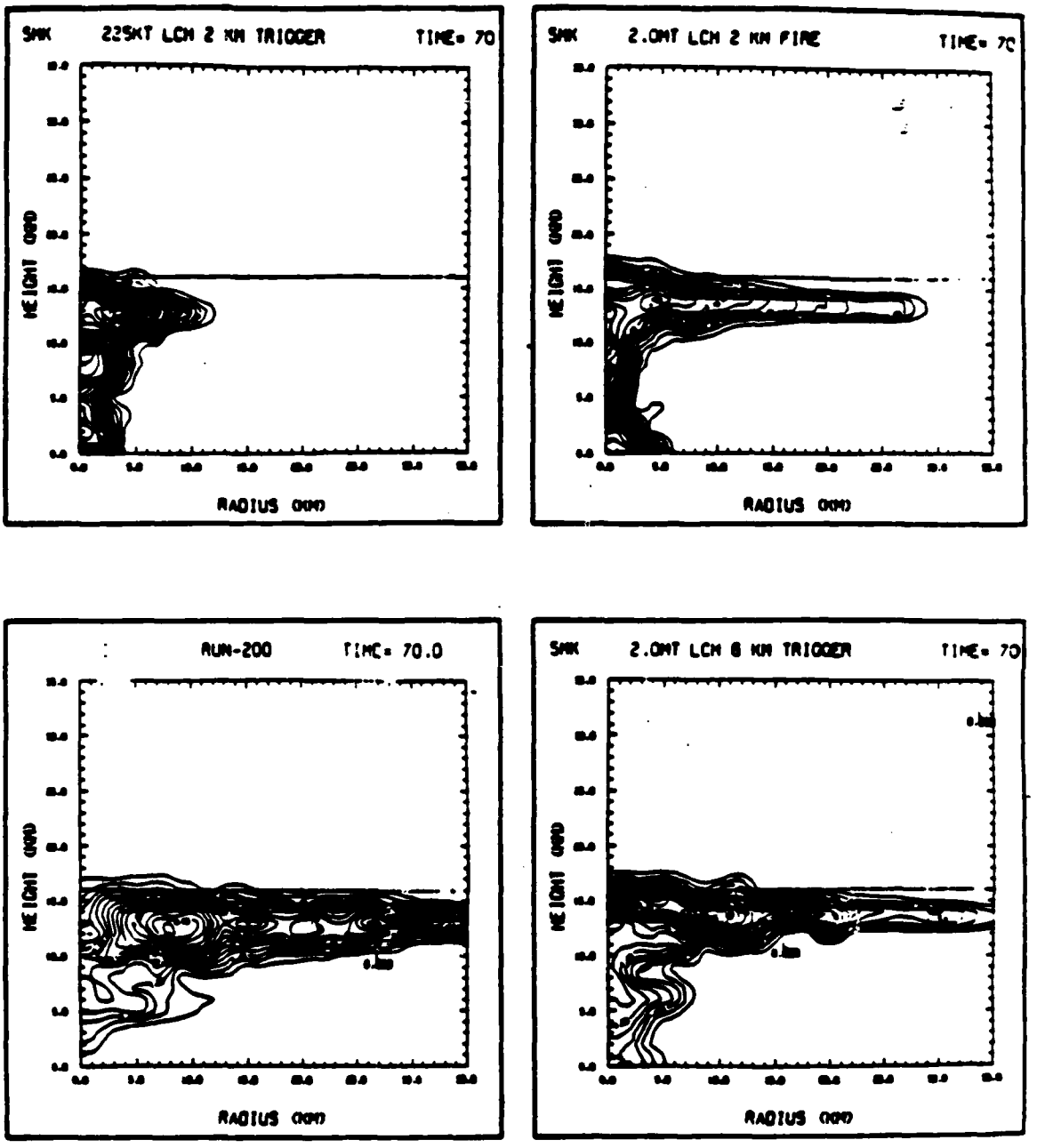

Figure 8. Comparison of smoke contours for 4 fires: a 2 km triggering fire (top left); a 6 km triggering fire (bottom right); a 2 km 1 hour fire (top right) and a 10 km triggering fire (bottom left).

Conclusions: The major conclusions that we have drawn from this series of simulations are:

(1) The ambient meteorology plays a dominant role in the atmospheric response.

(2) Given identical source total power, independent of spatial distribution (at least over a 10 km scale size area), the atmospheric response will be similar.

(3) The ambient moisture is a key parameter -- its presence allows the cloud to equilibriate at and above the tropopause; its absence results in a very low (sub-tropopause) stabilization height.

(4) Scavenging physics must be considerably improved. Total condensation can exceed 10^{14} g; total precipitation can surpass 10^{9} g.

SECTION 5
CONCLUSIONS

The overall conclusions which we draw from our simulations of the atmospheric response to both rising thermal bubbles (fireballs) and large area heat sources (large area fires) are:

(1) Considerably more work must be done to investigate the role of the ambient meteorology in understanding both fireball rise and the atmospheric response to large-area fires.

(2) The details of the ambient sounding over and above the simple analysis of the altitude of the tropopause do affect the cloud dynamics.

(3) The water vapor plays a very important role in the cloud dynamics. Without it, the plume from a large-area fire does not reach the tropopause; with it, a significant amount of precipitation occurs which may result in some level of scavenging of any injected particulates.

In addition to the above conclusions, we have identified certain areas of further research:

(1) Three-dimensional simulations. In both fireball rise and the cloud dynamics of large-area fires, the effect of wind shear needs to be identified. In the case of the large-area fires, the effect of the winds may increase the altitude of injection if the additional entrainment caused by the winds is less than the damping the flow currently feels due to the precipitation occurring over the heat source.

(2) Scavenging. The large amount of precipitation which we observe in our simulations of both the fireball rise and large-area fires may provide a great deal of scavenging of particulates.

These research areas are among those undergoing current study.

PAGES 22 THROUGH 36 ARE DELETED.